Pergamon

Int. J. Heat Mass Transfer. Vol. 40, No. 1, pp. 179–190, 1997

0017–9310/97 $15.00 + 0.00

PII: S0017–9310(96)00016–6

Hydrodynamics and heat transfer of wavy thin film flow

S. JAYANTI† and G. F. HEWITT‡

Department of Chemical Engineering, Imperial College of Science, Technology and Medicine, London SW7 2BY, U.K.

(*Received* 18 *October* 1993 *and in final form* 11 *September* 1995)

Abstract—The hydrodynamics and heat transfer of thin film flow with a wavy interface has been studied using computational fluid dynamics techniques. The velocity and temperature fields are obtained for periodic laminar flow with an assumed interface shape. The effect of sinusoidal and solitary waves on the heat transfer across the film is investigated. It is shown that the overall heat transfer coefficient is determined mainly by conduction through the film, rather than by the recirculation, if any, under the waves. However, the presence of interfacial waves still enhances the heat transfer coefficient due, mainly, to the effective thinning of the film. Copyright © 1996 Elsevier Science Ltd.

1. INTRODUCTION

The flow of a thin liquid film down a solid wall can often be observed in everyday life, as when rain water flows down a window pane. It is also a subject of industrial importance involving heat transfer and mass transfer, typical examples of which are film cooling of turbine blades and gas absorption in wetted-wall columns, respectively. There have been a number of studies of falling films over the past several decades. One of the earliest of these is that of Nusselt [1] dealing with steady laminar flow in a smooth condensate film flowing down a vertical wall under the action of gravity. He obtained the following expressions for the film thickness (δ), average liquid velocity in the film (u_a) and the average heat transfer coefficient (λ) in terms of Q, the volumetric liquid flow rate per unit wetted perimeter:

$$\delta = \left[\frac{3\nu}{g}\right]^{1/3} Q^{1/3} = \left[\frac{3\nu^2}{g}\right]^{1/3} Re^{1/3} \quad (1a)$$

$$u_a = \left[\frac{g}{3\nu}\right]^{1/3} Q^{2/3} = \left[\frac{\nu g}{3}\right]^{1/3} Re^{2/3} \quad (1b)$$

$$\lambda = \frac{k}{\delta} = \left[\frac{k^3 g}{3\nu}\right]^{1/3} Q^{-1/3} = \left[\frac{k^3 g}{3\nu^2}\right]^{1/3} Re^{-1/3}, \quad (1c)$$

where g is the acceleration due to gravity, k the thermal conductivity of the fluid, ν its kinematic viscosity, and Re is the film Reynolds number defined as $u_a\delta/\nu$.

The above relations are valid for a smooth film. However, it is well-known (see for example, the review by Fulford [2]) that waves are formed on the surface of the film, even for small liquid flow rates. Linear stability analyses by several researchers have shown that a smooth film is unstable for film Reynolds numbers greater than a critical value. For the free flow of water down a vertical wall, the critical value was put at about 6 by Kapitza [3, 4], while Benjamin [5] found that vertical film flow was always inherently unstable, although the instability may not be physically manifest at very low Reynolds numbers. The analyses of other workers [6, 7] also show a similar trend [2]. The instability of the smooth film has also been confirmed experimentally by several researchers [2, 8–10] who reported the onset of wavy motion for Reynolds numbers less than 10. The wave patterns on falling films are many and varied, and have been studied over a number of decades; useful reviews can be found in Dukler and Bergelin [11] and Fulford [2]. The main results from these studies are as follows. Below the critical Reynolds number for wave inception, the film surface is completely smooth. At Reynolds numbers slightly higher, small, symmetrical waves appear. At still higher flow rates, the regular symmetrical waves become asymmetrical and steepen at the front and have a gently sloping tail. These 'roll' waves are not regular, and may interact with each other. These waves, which range in amplitude from two to five times the substrate thickness, carry a large fraction of the total liquid mass, and are thought to control the rate of heat and mass transfer rates [12]. There may also be smaller capillary waves in between successive roll waves. At still higher flow rates, the wave pattern becomes chaotic and the flow appears to be turbulent. This happens at a Reynolds number in the region of 250–400, although much higher values have been reported for this transition. In a typical falling film, the interface would be smooth for a short distance

†Now at the Indian Institute of Technology, Madras, India.

‡Author to whom correspondence should be addressed.

NOMENCLATURE

g	acceleration due to gravity	u_a	average velocity in film
k	thermal conductivity	u_w	wave velocity
L_t	length of tail section	v	velocity normal to wall (y-direction)
L_f	length of wave front section	x	distance down film.
Pr	Prandtl number		
Q	volumetric liquid flow rate per unit wetted perimeter	Greek symbols	
Re	film Reynolds number ($U_a\delta/\nu$)	δ	liquid film thickness
$T_i(x)$	interface temperature at position x	λ	average heat transfer coefficient
$T_w(x)$	wall temperature at position x	$\lambda(x)$	local heat transfer coefficient
u	velocity down film (x-direction)	ν	kinematic viscosity.

from the entry, followed by the inception and rapid growth of sinusoidal waves leading to the formation of the irregular roll waves [13, 14, 40]. The statistical characteristics of the interfacial waves have been reported, among others, by Dukler and co-workers [15–17], and more recently by Karapantsios *et al.* [18].

There have been several theoretical studies of the hydrodynamics of the wave motion in falling films. These range from the Orr–Sommerfeld type of linear stability analyses to computer simulation of wavy film flow [3–5, 14, 19–25]. The earlier studies concentrated on obtaining the frequency and velocity of sinusoidal waves, and are limited to small Reynolds numbers. The more recent studies focused on obtaining the velocity field, etc. for the roll waves. Although some streamlines and velocity fields have been obtained, especially for roll waves (see, for example [refs. 20, 23–26]), the effect of the waves on heat and mass transfer has not been systematically investigated, in spite of the well-established fact that experimental studies have shown that the transport processes are strongly affected by the presence of waves. For example, Kirkbride [27] reported heat transfer data in falling film condensation which showed a 25–50% increase in the heat transfer coefficient over that predicted by the Nusselt smooth film theory. Similarly, Bays and McAdams [28] reported a 20–30% increase in heat transfer coefficient for the heating of fluids in falling film towers. More recently, Kutateladze and Gogonin [29] and Chun and Seban [30] present data for the two cases confirming that the heat transfer coefficient in wavy laminar flow is higher than that predicted by the Nusselt equation. The case for the wave effect on mass transfer has also been made by several researchers including Emmert and Pigford [31] and Stirba and Hurt [32], both of whom reported a manyfold increase (over the smooth-film theory) of mass transfer coefficient for wavy films. More conclusive evidence is presented by Brauner and Maron [33] who measured the local instantaneous values of film thickness and mass transfer rate in inclined falling film flow.

While the enhancement of heat and mass transfer coefficient by interfacial waves is thus established, the reason why and how this happens is not clear. It has been suggested that this may be due to the increase in interfacial area due to rippling, but this possibility has been discounted by the experimental results of Portalski and Clegg [34]. Other reasons, such as increased bulk mixing by the waves and the thinning of the film due to the waves, have also been proposed to account for the increase in heat transfer coefficient under wavy flow conditions. The purpose of the work described in this paper is to investigate the hydrodynamics of the flow, with a view to understanding the role of the interfacial waves in heat transfer across the film. This is done numerically by calculating the velocity and temperature fields in wavy flow using computational fluid dynamics (CFD) techniques. The calculation methodology is described in Section 2 and the results are discussed in Section 3.

2. CALCULATION METHODOLOGY

Numerical simulation of fluid flow is increasingly being used to solve a wide variety of fundamental and practical fluid flow problems. Here, the set of equations governing the fluid flow (comprising normally mass and momentum conservation equations with appropriate boundary conditions) is solved using spectral or finite element or finite difference methods. The techniques have been developed to such an extent that normally they take the form of CFD codes, some of the well-known examples of which are TRAC, PHOENICS, FLOW3D and FLUENT. In the present study, the flow field calculations are performed using the Harwell-FLOW3D computer program developed at the Harwell Laboratory of the UKAEA [35]. FLOW3D uses a finite volume method-based discretization of the governing partial differential equations on a nonorthogonal body-fitted grid. It adopts the nonstaggered grid approach, whereby the values of all the variables are evaluated at the centres of the cells (unlike in the case of the staggered grid approach where fluxes are evaluated at cell faces) and uses the Rhie–Chow algorithm [36] extended to three dimen-

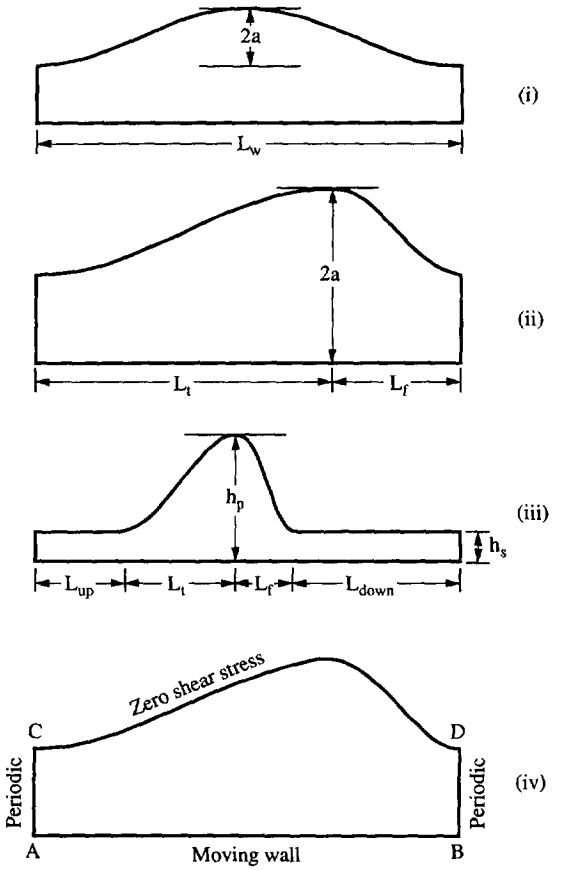

Fig. 1. Various shapes of the falling film interface: (i) with a sinusoidal wave; (ii) with a distorted sinusoidal wave; and (iii) with a solitary roll wave. (iv) Boundary conditions on flow domain.

sions [37] to overcome the problem of chequerboard oscillations in velocity and pressure usually associated with the use of nonstaggered grids. In the present study, the SIMPLEC algorithm [38] is used for pressure–velocity decoupling. Details of the computer program can be found in Jones *et al.* [35] and Burns and Wilkes [37].

2.1. *Specification of the problem*

In the present study, calculations of velocity and temperature fields in wavy flow have been performed. Three types of wave shapes have been used in the calculations; these are regular sine waves [Fig. 1(i)]; distorted sine waves in which the wave front is steeper than the tail of the wave [Fig. 1(ii)]; and solitary or roll waves in which a wave form flows over a substrate of constant thickness [Fig. 1(iii)]. All three types of waves are encountered in falling film flow, and the velocity field in the third type of wave has been calculated earlier by other researchers, for example, Wasden and Dukler [24, 25] and Maron *et al.* [23], although the focus of their studies was different from that of the present study. In as much as the waves are assumed to be periodic, the time dependence of the problem has been removed by taking a frame of reference moving at the velocity of the wave. Thus, a steady, laminar flow through the flow domains, shown in Fig. 1, is simulated. Since the wave moves downwards at a constant velocity u_w in a stationary frame of reference, the boundary condition on the wall [side AB in Fig. 1(iv)] is specified as $u = -u_w$ and $v = 0$, where u and v are the velocities in the x- and y-directions. In view of the periodicity of the wave, plane AC and BD are specified as periodic planes. This means that the velocity and temperature profiles across the two planes are identical (but they need not correspond to those of fully developed flow). The presence of gas beyond the interface (side CD) is neglected, and the boundary condition on this side is that there is no shear stress at the interface. For the temperature field, sides AC and BD are again assumed to be periodic while there is a constant heat flux into the flow domain from the interface (side CD) and the same amount of heat flux going out of the flow domain at the wall (side AB). This would correspond to the case of condensation heat transfer. For convenience, constant properties are assumed for the fluid with the density being 1000 kg m^{-3}, dynamic viscosity 0.001 kg m^{-1} s^{-1}, specific heat 1 J kg^{-1} and thermal conductivity 0.001. It should be noted that the density and the viscosity correspond to those of water while the Prandtl number, Pr, is equal to 1.

2.2. *Grid independence*

The accuracy of the solution obtained from the CFD calculations depends on a variety of factors, including the complexity of flow field and the accuracy of the numerical solution. In the present case, the flow is laminar and steady and the geometry is fairly simple. This means that the closure problem in turbulence modelling can be avoided, and an accurate solution can be obtained with a fine enough grid. With this in view, several grids of increasing refinement were tried for the case of Fig. 1(a). A body-fitted grid of the type shown in Fig. 2 was fitted with 20×10, 20×15, 20×20, 40×20, 40×40 and 80×40 points in the x- (flow direction) and the y-directions, respectively. Calculations were performed for a typical case. It was found that satisfactory solutions could be obtained with a grid as small as 20×20. This is probably due to the use of a higher order (nominally second-order accurate) upwinding scheme [39] for the discretization of the convective term in the momentum equations. The results reported here were obtained using this or a finer grid.

2.3. *Determination of the wave velocity*

In the present study, the flow field was calculated for a wave of specified shape, i.e. for given amplitude, wave length, mean film thickness and distortion, if any. It has been mentioned in Section 2.1 that one of the boundary conditions on the wave was that the wall moved at the wave velocity, u_w, in a countercurrent flow direction. This velocity is not known *a priori* and is calculated as part of the solution. For a

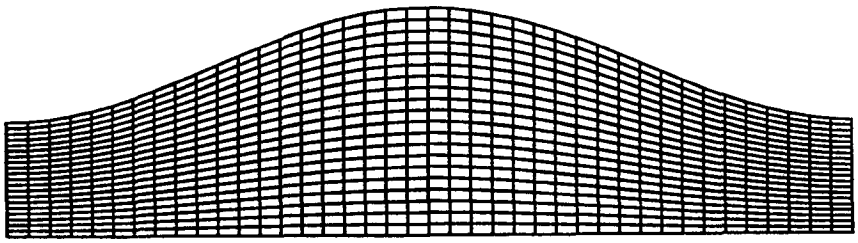

Fig. 2. Typical grid for the flow domain.

given mean film thickness and the shape of the interface, the flow field is first calculated with an estimated value of the wave, and hence, the wall velocity. Since the forces acting on the flow are the gravitational force and the shear stress at the wall (the interfacial shear stress being zero by assumption), these two should balance each other when integrated over the entire wave. However, this need not be so if the wave velocity is chosen incorrectly. This is then used as the criterion to determine the correct wave velocity. A typical variation with wall velocity of the ratio of the overall wall shear stress to gravitational force is shown in Fig. 3. The wave velocity which gives the ratio to 1.000 ± 0.001 was taken as the true wave velocity. A procedure similar to this was used by Wasden and Dukler [24, 25] in their calculations of the flow field in solitary roll waves. Their criterion was based on the pressure being zero at the outlet cross-section, the argument there being that it would be so for a non-accelerating film. Such a criterion would not be applicable for periodic flows.

The solution corresponding to the true wave velocity gives the velocity and the temperature field for the laminar, steady flow of a fluid flowing with the specified position and shape of the interface. From the known velocity field and the average thickness (averaged over the wavelength) of the film, $\bar{\delta}$, the average film velocity in a stationary frame of reference, $\bar{u}_a$, can be calculated. The Reynolds number of the flow is then calculated as $Re = \bar{u}_a \delta / \nu$. The local heat transfer coefficient is determined as $\lambda(x) = q(x)/[T_i(x) - T_w(x)]$, where $q(x)$ is the heat flux at position x, $T_i(x)$ the interface temperature and $T_w(x)$ the wall temperature at the same x position. The average heat transfer coefficient is obtained by averaging the local value over the wavelength. This Reynolds number is then used to quantify the wave-induced enhancement of the heat transfer coefficient.

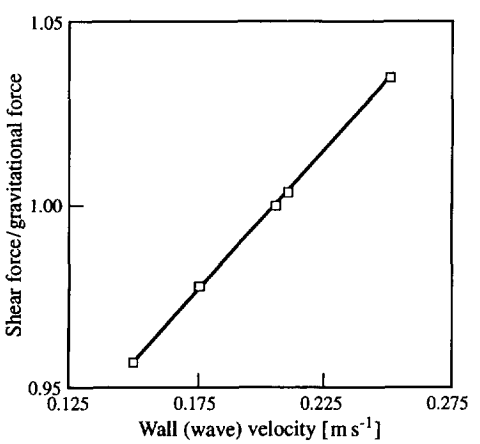

Fig. 3. Relation between the wall velocity and the ratio $\bar{\tau}_w/\rho g \bar{h}$ illustrating the dependence between the imposed wall (wave) velocity and the wall shear stress obtained from calculation.

The calculation methodology described above has been used to determine the flow field for a range of flow variables. The results from these calculations are described in the next section.

3. RESULTS

The results of the calculations for falling films without interfacial waves are shown first in Table 1. In these cases, a constant film thickness was assumed, and the motion of liquid under the action of gravity was calculated subject to a specified wall velocity. The average flow velocity, interface velocity and the heat transfer coefficient obtained from the calculation are listed in the table. The results, when converted into a stationary frame of reference, are independent of the wall velocity (unlike in the case shown in Fig. 3). It is noted that perfect agreement with theory is obtained for this simple, one-dimensional flow in all the cases. The results in the more complicated case of a film with a wavy interface are presented below in three parts. The first part deals with the calculations of sinusoidal waves of the type shown in Fig. 1(i); the second with distorted sine waves of the type shown in Fig. 1(ii); and the third part with solitary roll waves of the type shown in Fig. 1(iii).

3.1. *Sinusoidal waves*

For this case, the wavelength is taken as 10 mm, which is typical for the flow of water down a pipe [40]. Several cases were run in which a regular sine wave of amplitude of 10% of the film height was assumed to be present on a film of thickness varying between 0.05 and 0.5 mm. The film thickness would correspond to a smooth film Reynolds varying between 0.4 and 409. The waves themselves would correspond to the long-wave approximation made in linear stability analyses. The methodology described in Section 2.3 was used to calculate the wave velocity in each case.

Typical results from these calculations are shown in Fig. 4, which shows the velocity contours and the

Table 1. Smooth falling film calculations: density = 1000 kg m^{-3}, viscosity = 0.001 kg m^{-1} s^{-1} and thermal conductivity = 0.001 W m^{-1} K^{-1}, $Pr = 1$

δ [mm]	u_a [m s^{-1}]	$Re = u_a\delta/\nu$	λ [W $m^{-2}.K^{-1}$]	$u_i u_a$	λ/λ_{th}
0.05	0.00819	0.41	20.00	1.50	1.00
0.10	0.0327	3.27	10.00	1.50	1.00
0.15	0.0736	11.04	6.667	1.50	1.00
0.225	0.1656	37.26	4.444	1.50	1.00
0.30	0.2944	88.32	3.333	1.50	1.00
0.40	0.5232	209.3	2.500	1.50	1.00
0.50	0.8174	408.7	2.000	1.50	1.00

temperature contours for the case of mean film thickness of 0.1 mm corresponding to a smooth film Reynolds number of 3.27. (The wave shape is foreshortened to bring out the variation more clearly, but the actual wavelength to amplitude ratio is 1000.) It can be seen that nearly symmetric velocity and temperature fields are obtained for this case. There is no evidence of recirculation under the wave crests. At higher Reynolds numbers (corresponding to larger film thicknesses), the symmetry is maintained, but a phase shift appears between the film thickness and the flow variables. This is illustrated in Fig. 5 which shows the variation of the normalized wall shear stress and the normalized heat transfer coefficient along the wave as a function of the film thickness. (The wave amplitude to film thickness ratio in all cases is kept at 0.1.) The sinusoidal interface profile gives rise to a sinusoidal perturbation in the wall shear stress in all cases. However, except at very low Reynolds numbers, the distribution is not symmetrical about the midpoint, and a phase shift appears. Another noticeable feature is that the amplitude of the wall shear stress variation increases with Reynolds number, although the response remains linear in the sense that it consists of the single, fundamental harmonic associated with the wave shape.

The results obtained in this series of calculations are summarized in Table 2. Here, the wave velocity and the average flow velocity obtained for each case are given. It is seen that the ratio of the wave velocity

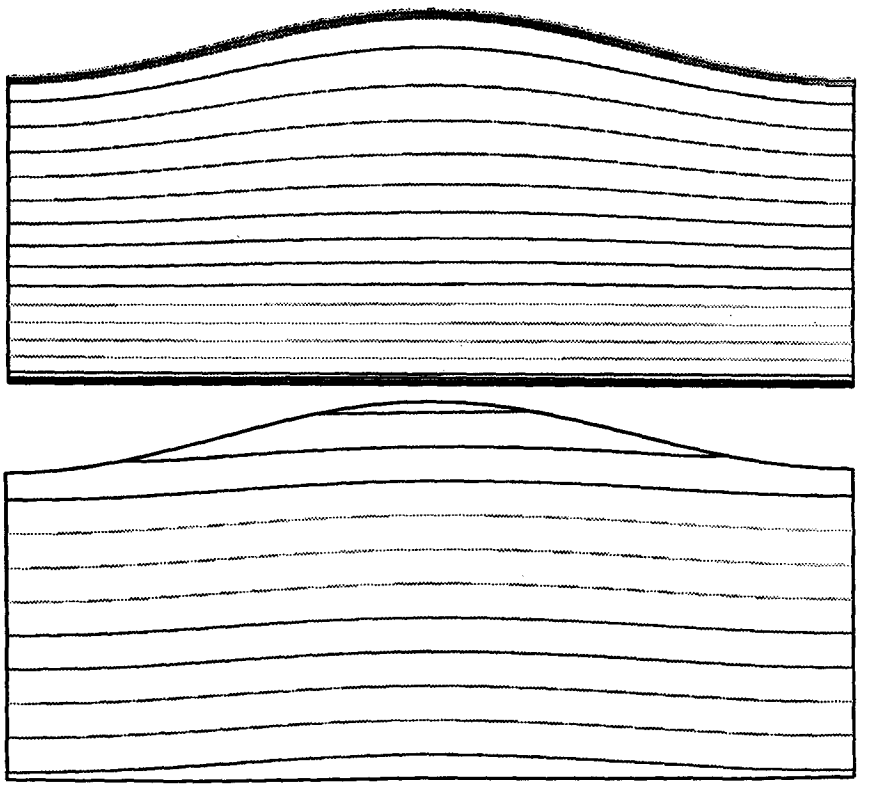

Fig. 4. Results obtained for the case of a mean film thickness of 0.1 mm corresponding to a smooth film Reynolds number of 3.27: (i) axial velocity contours, and (ii) temperature contours. The amplitude to wavelength ratio is 0.1.

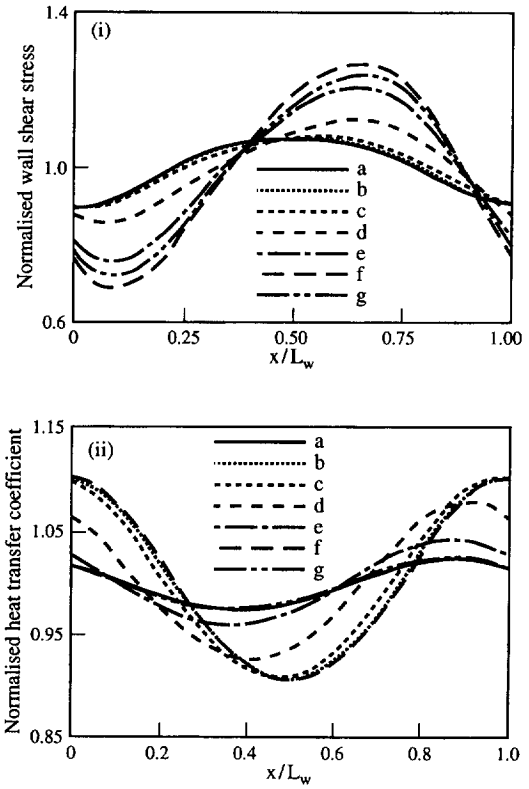

Fig. 5. Variation of (i) normalized wall shear stress and (ii) normalized heat transfer coefficient along the wave at a mean film thickness of (a) 0.05 mm, (b) 0.1 mm, (c) 0.15 mm, (d) 0.225 mm, (e) 0.3 mm, (f) 0.4 mm and (g) 0.5 mm. The wall shear stress and the heat transfer coefficient were normalized by dividing by the mean value over the wave.

to the average flow velocity approaches the theoretical value of 3 only at very low Reynolds numbers, and that it decreases with increasing Reynolds number. The average flow velocity in wavy flow is slightly greater than that for a smooth film flow, but the effect is very small. Although the local heat transfer coefficient varies appreciably over the wave, the wavelength-averaged value is only slightly higher (by less than 1%) than the smooth film value. Thus, small amplitude, long-wavelength sinusoidal waves do not have a significant effect on the heat transfer.

The effect of increasing wave amplitude is summarized in Table 3 and Fig. 6 for a mean film thickness of 0.1 mm and a wave amplitude of 0.1, 0.2, 0.333 and 0.5 of the mean film thickness. It is seen from the table that the wave velocity decreases as the amplitude increases. There is a more pronounced increase in the mean flow velocity through the wave. Examination of the velocity field showed that there was no recirculation in the wave crest in the first three cases, while a weak recirculation zone could be seen in the fourth case with a wave amplitude of half of the mean film thickness. The variation of the wall shear stress is symmetrical in all cases [Fig. 6(i)]; however, a higher harmonic variation occurs in the last two cases, thus illustrating the departure from linear response. The variation of the local heat transfer coefficient [Fig. 6(ii)] is sinusoidal and symmetrical in all cases. This is due to the fact that the heat transfer process is dominated by thermal conduction through the film, rather than by convection effects. Indeed, the local heat transfer coefficient is found to be closely approximated by the Nusselt's smooth film expression if the local film thickness is used to evaluate it. It may therefore be argued that there is no enhancement of heat transfer in wavy flow. However, wavy flow has an effect on the hydrodynamics of the flow; for example, the mean flow velocity is higher than what it would be for a smooth film of the same mean film thickness, and this fact must be taken into account in assessing the wave-induced enhancement. This can be done as follows.

The Reynolds number of the flow based on the mean flow velocity and the mean film thickness can be calculated for each case. This then would be the Reynolds number of the flow corresponding to the assumed interface shape. The wave-induced enhancement can then be quantified by comparing the calculated heat transfer coefficient with that obtained in smooth film flow with the same Reynolds number, which, of course, is given by equation (1c) above. The ratio of these two quantities is given in Table 3, and is seen to increase from 1.010 to 1.276 as the amplitude-to-height ratio increases from 0.1 to 0.5. Thus, there would be an appreciable enhancement in the heat transfer rate in the presence of large amplitude sinusoidal waves, even without a significant recirculation under the wave crest.

Table 2. Effect of small-amplitude sinusoidal waves on thin falling film flow: same fluid properties as in Table 1, and amplitude/film thickness = 0.1

δ [mm]	L_w [mm]	u_w [m s^{-1}]	u_a [m s^{-1}]	$Re = u_a\delta/\nu$	λ [W m^{-2} K^{-1}]	u_w/u_a	λ/λ_{th}
0.05	10	0.0232	0.0083	0.414	20.00	2.801	1.010
0.10	10	0.0925	0.0331	3.31	10.00	2.794	1.009
0.15	10	0.207	0.0745	11.18	6.667	2.777	1.009
0.225	10	0.460	0.1674	37.67	4.444	2.748	1.009
0.30	10	0.800	0.2963	88.89	3.333	2.700	1.007
0.40	10	1.30	0.5250	210.0	2.500	2.476	1.006
0.50	20	1.92	0.8199	410.0	2.000	2.342	1.006

Table 3. Effect of increasing wave amplitude on wavy film flow; mean film thickness = 0.1 mm, wave length = 100 mm

a/δ [mm]	u_w [m s^{-1}]	u_a [m s^{-1}]	$Re = u_a\delta/\nu$	λ [W m^{-2} K^{-1}]	u_w/u_a	λ/λ_{th}
0.1	0.095	0.0332	3.315	10.05	2.866	1.010
0.2	0.095	0.0346	3.455	10.20	2.750	1.039
0.333	0.092	0.0376	3.764	10.60	2.444	1.111
0.5	0.0845	0.0442	4.419	11.54	1.912	1.276

3.2. *Distorted sinusoidal waves*

It is known from experiments that after inception, the sinusoidal waves grow with distance, and also distort such that they have a steeper front and a longer tail. The hydrodynamics of these waves has been investigated using the same methodology as above using an asymmetric interface shape of the type shown in Fig. 1(ii). Calculations were performed for a mean film thickness of 0.3 mm (corresponding to a smooth film Reynolds number of 88.3) and an amplitude of 0.1 mm. The distortion of the sinusoidal wave can be characterized by a distortion factor defined as the ratio of the length of the wave tail section [L_t in Fig. 1(ii)] to that of the wave front section (L_f). When the ratio is unity, the wave is symmetrical, and the higher the ratio is, the more the distortion. (The ratio can also be less than one implying that the wave tail is steeper than the front, but this is unphysical, and the possibility is not considered here.) In the calculations, the distortion factor is varied between 1 and 4. The results are summarized in Table 4 and Fig. 7. As the distortion increases and the wave front steepens, the wave velocity decreases significantly, while the mean flow velocity decreases by a much smaller factor. This is in contrast to the case of increasing wave amplitude where the mean flow velocity increases as the wave velocity decreases (see Table 3). This is reflected in the wall shear stress variation shown in Fig. 7(i), which becomes more uniform as the distortion increases. The local heat transfer coefficient follows closely the inverse of the film thickness, although there is some deviation. While the wavelength-averaged heat

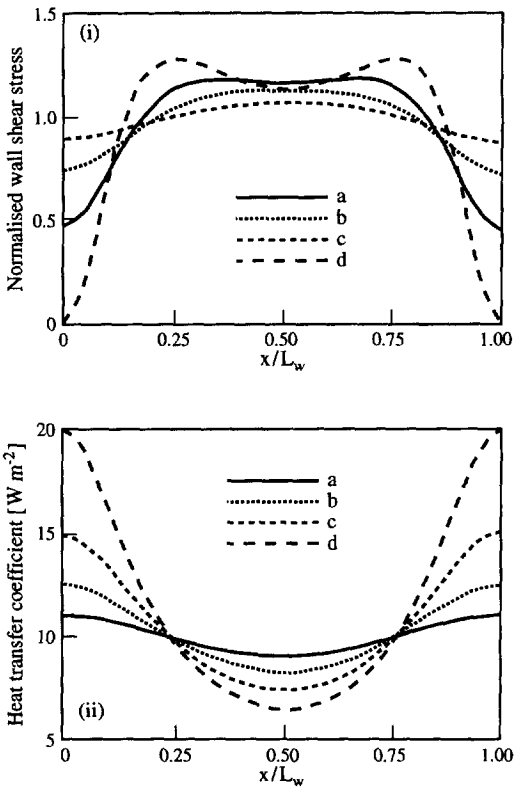

Fig. 6. Variation of (i) normalized wall shear stress and (ii) normalized heat transfer coefficient along the wave at a mean film thickness of 0.1 mm and an amplitude to film height ratio of (a) 0.1, (b) 0.2, (c) 0.333 and (d) 0.5. The wall shear stress and the heat transfer coefficient were normalized by dividing by the mean value over the wave.

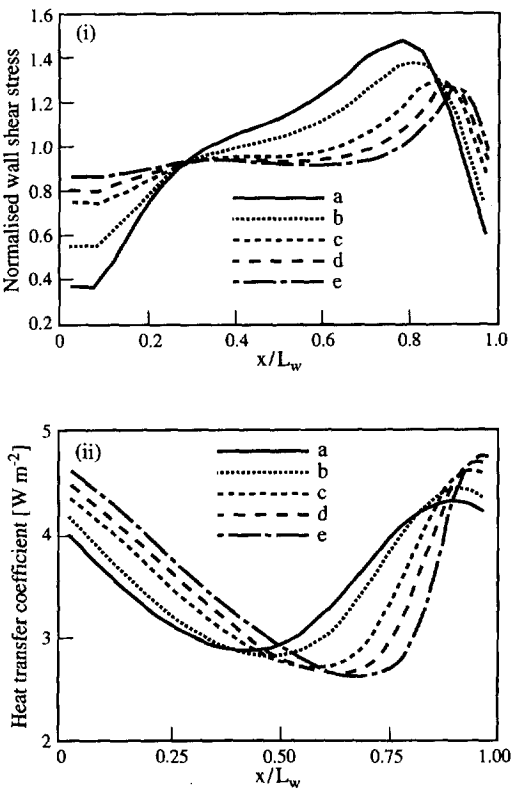

Fig. 7. Variation of (i) normalized wall shear stress and (ii) heat transfer coefficient along the wave at a mean film thickness of 0.3 mm and an amplitude of 0.1 mm for a distortion factor of (a) 1.22, (b) 1.5, (c) 2.5, (d) 3.0, and (e) 4.0. The wall shear stress was normalized by dividing by its mean value over the wave.

Table 4. Effect of distortion of the sinusoidal wave on wavy film flow; mean film thickness = 0.3 mm, wave length = 100 mm; $a/\delta = 0.333$

L_t/L_f	u_w [m s^{-1}]	u_a [m s^{-1}]	$Re = u_a\delta/\nu$	λ [W m^{-2} K^{-1}]	u_w/u_a	λ/λ_{th}
1.0	0.745	0.316	94.92	3.516	2.355	1.081
1.22	0.657	0.306	91.80	3.537	2.147	1.075
1.5	0.604	0.299	89.82	3.563	2.017	1.075
2.5	0.538	0.291	87.15	3.619	1.852	1.081
3.0	0.512	0.287	86.01	3.648	1.786	1.085
4.0	0.490	0.283	84.99	3.676	1.730	1.089

transfer coefficient increases with increasing distortion, the overall enhancement in terms of the equivalent Reynolds number smooth film flow is nearly the same as for a corresponding sinusoidal wave (see Table 4).

3.3. *Solitary or roll waves*

Solitary or roll waves [see Fig. 1(iii)] are much larger—both in amplitude and in wavelength—than the sinusoidal waves considered above [17]. Typically, they have an amplitude of several times the base film (substrate) thickness. These are solitary waves in the sense that any significant variation of amplitude is confined to one or two centimetres in the flow direction, while successive waves are separated by a distance of several centimetres. The hydrodynamics of such waves have been studied to some extent by Dukler and co-workers [12, 24, 25] and Maron and co-workers [22, 23], although the associated heat transfer problem has not been addressed before. Here, we present the velocity and temperature fields for three cases for which the interface height, $h(x)$, is given as follows:

$$h(x) = \frac{1}{2}\left[(h_p + h_s) - (h_p - h_s)\cos\frac{\pi x}{L_t}\right] \quad \text{for } 0 \leqslant x \leqslant L_t$$

$$= \frac{1}{2}\left[(h_p + h_s) - (h_p - h_s)\cos\frac{\pi(x - L_t)}{L_f}\right] \quad \text{for } L_t \leqslant x \leqslant L_t + L_f$$

$$= 0 \quad \text{for } x < 0 \quad \text{or } x > L_t + L_f, \tag{2}$$

where h_p is the peak height of the wave, h_s the substrate thickness, L_f the length of the front section of the wave, L_t that of the tail section and x_p the x-position at which the wave height is the maximum [see Fig. 1(iii)].

The wave characteristics for the three cases are given in Table 5. Note that all the three waves are asymmetrical and have a steeper front, and the peak-to-substrate ratio varies from 2 to 6. The length between successive waves is taken to be 10 cm, and periodic boundary conditions are imposed at the two ends. It is mentioned in passing that these waves are similar to those studied by Maron *et al.*, although the boundary conditions appear to be different.

The results of the calculations for the three cases are summarized in Fig. 8 and in Table 6. Figure 8(i) shows the streamfunction contours and the temperature contours. (As before, the waves are foreshortened, and the wave slopes are not as steep as they appear.) It can be seen from the streamfunction plot that there is no recirculation under the wave in the first case, while there is a large recirculation zone in the last two cases. One can therefore expect a corresponding enhancement in heat transfer rate in the last two cases. Indeed, the temperature contours given in Fig. 8(ii) show that there is a convective effect on the temperature distribution. The extent of the effect can be gauged from the local heat transfer coefficient variation shown in Fig. 9. Here, corresponding to each case are drawn two curves: one showing the actual heat transfer coefficient (defined as the local heat flux divided by the local temperature difference between the interface and the wall), and the other showing the heat transfer coefficient if it were entirely due to thermal conduction alone (which is given by the thermal conductivity divided by the local film thickness, the variation of which is also shown in the figure). It can be seen that, in all the cases, the heat transfer coefficient in the wave is much less than that in the thin film outside the wave, showing that the heat transfer

Table 5. Characteristics of the solitary waves investigated

Case	h_s [mm]	h_p/h_s	L_f [mm]	L_t [mm]	L_{up} [mm]	L_{down} [mm]
1	0.1438	2	12.08	28.18	18.0	39.0
2	0.1438	4	12.08	28.18	18.0	39.0
3	0.1438	6	12.08	28.18	18.0	39.0

process is still dominated by thermal conduction. In the first case, where there is no recirculation under the wave, the two curves are nearly identical. The effect of recirculation in the wave can be seen to some extent in case 2, and more clearly in case 3, in which the heat transfer coefficient in the wave tail is clearly above the value obtained by conduction alone. There is a corresponding, but smaller decrease in the heat transfer coefficient in the wave front. The variation of the heat transfer coefficient is no longer the same as that of the inverse of the film thickness.

The overall effect of convection on the heat transfer coefficient can be obtained by calculating the average heat transfer coefficient in the wave and comparing it with that obtained due to conduction alone (i.e. average value of k/δ). These values are given for the three cases in Table 6. When averaged over the wave region only, there is virtually no enhancement due to convection in the first case while it is more than 10% in the third case. When considered over the wave and the substrate film, the recirculation-induced enhancement is very small, of the order of a few per cent, even in the third case. This shows that the overall heat transfer rate in thin film flow is not improved significantly by recirculation under the waves.

The effective enhancement of the heat transfer coefficient can be calculated as before by comparing with the heat transfer coefficient obtained in a smooth film flow at the same Reynolds number. These calculations are summarized in Table 7. It can be seen that increasing the amplitude of the wave increases

(i)

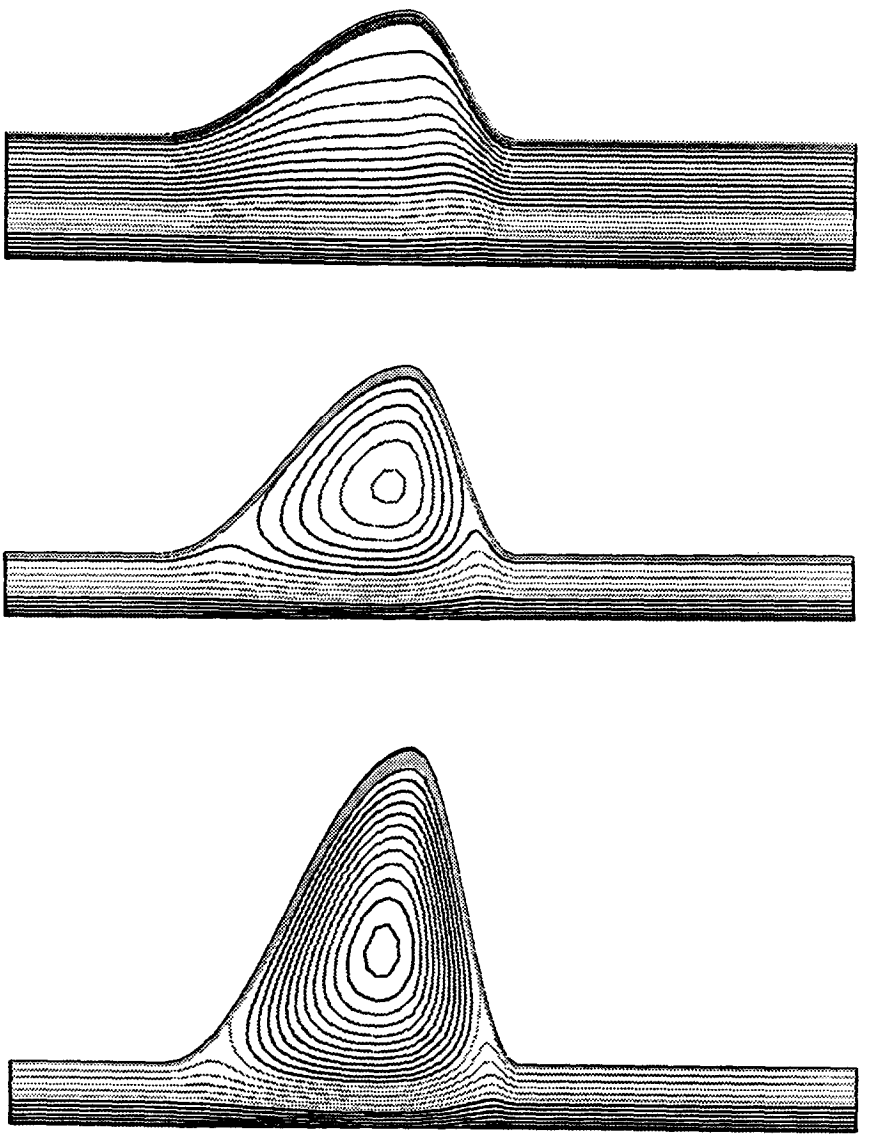

Fig. 8. Contours of (i) streamfunction and (ii) temperature for solitary waves for a peak to substrate film height ratio of (a) 2, (b) 4 and (c) 6. (*Continued overleaf.*)

(ii)

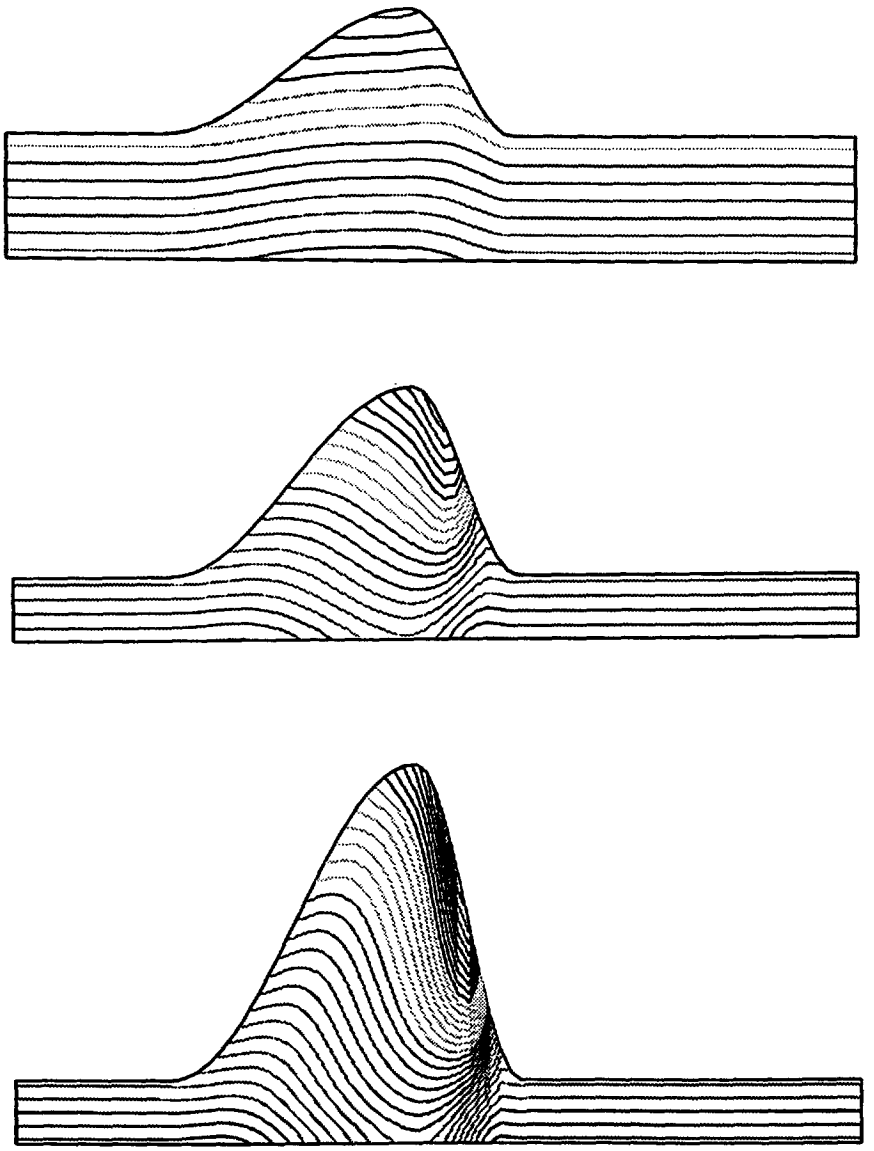

Fig. 8—(*Continued.*)

the average film thickness as well as the mean flow velocity. The resulting increase in Reynolds number more than offsets the decrease in heat transfer coefficient. Thus, an effective enhancement of nearly 35% is obtained in the third case.

4. DISCUSSION AND CONCLUSION

We have studied the hydrodynamics and heat transfer characteristics of a wavy laminar flow of given interface shape. The wave velocity and the velocity

Table 6. Heat transfer coefficients in the solitary wave calculations

Case	λ under wave only [W m^{-2} K^{-1}] calculated	λ under wave only [W m^{-2} K^{-1}] theory (conduction)	calc/theory	λ under wave and substrate [W m^{-2} K^{-1}] calculated	λ under wave and substrate [W m^{-2} K^{-1}] theory (conduction)	calc/theory
1	4.912	4.916	0.999	6.109	6.108	1.000
2	3.537	3.471	1.019	5.540	5.507	1.006
3	3.145	2.829	1.111	5.378	5.241	1.026

Table 7. Heat transfer enhancement in the solitary waves

Case	$\bar{\delta}$ [mm]	u_w [m s^{-1}]	$\bar{u}_a$ [m s^{-1}]	$Re = \bar{u}_a\bar{\delta}/\nu$	λ [W/m^{-2} K^{-1}]	λ_{th} [W m^{-2} K^{-1}]	λ/λ_{th}
1	0.1736	0.400	0.1225	21.27	6.109	5.356	1.141
2	0.2330	0.251	0.1497	34.89	5.540	4.452	1.220
3	0.2928	0.259	0.1772	52.07	5.378	3.974	1.353

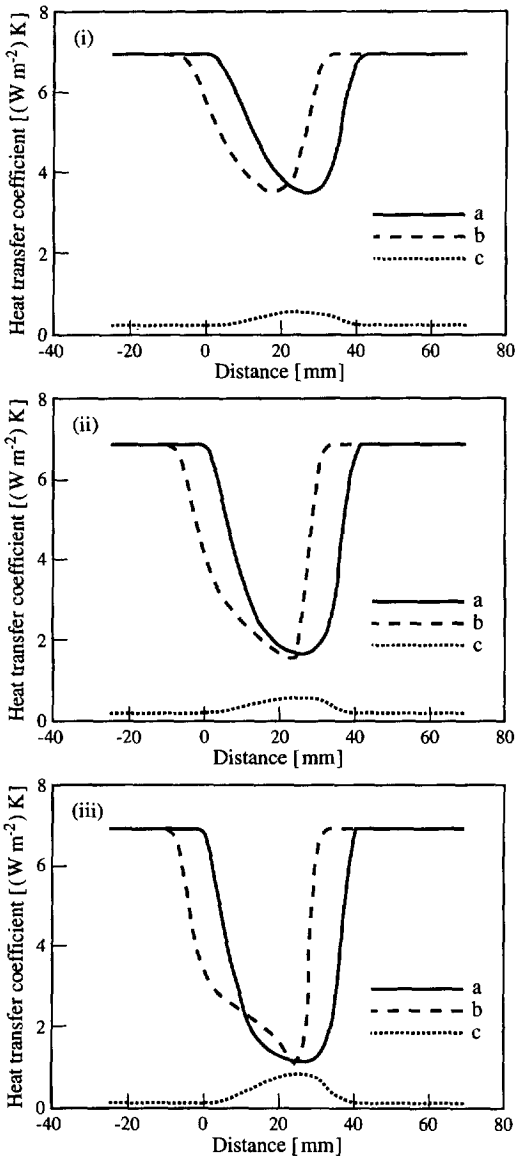

Fig. 9. Variation of the local heat transfer coefficient in the solitary wave calculations for a peak to substrate film height ratio of (i) 2, (ii) 4 and (iii) 6. Shown in the figures are (a) the theoretical heat transfer coefficient, (b) the calculated heat transfer coefficient and (c) the profile of the wave.

field were obtained such that there was a balance between the wall shear stress and the gravitational force. Note that the shape of the interface is not predicted as part of the solution, but that the solution obtained (subject to the conditions of periodicity and no interfacial shear) corresponds to the case of falling film flow if the interface had taken the shape assumed in the calculation. Three types of wave shapes commonly found in falling films were included in the study, and the emphasis was on the role of the interfacial waves on heat transfer across the film. In as much as the wavy flow hydrodynamics are not defined entirely by the mean film thickness (wave parameters such as amplitude, shape and wavelength also affecting the mean flow velocity), the concept of equivalent Reynolds number has been proposed as the basis for comparing a smooth film and a wavy film: the heat transfer enhancement in wavy film flow is determined by comparing its heat transfer coefficient with that expected (from Nusselt's theory) in a smooth film having the same film Reynolds number. The calculations were performed for steady state, and no account was taken of any evolution of the shape of the wave either with distance or with time. The underlying assumption is that any time-dependent evolution of the wave shape is slow enough so that the hydrodynamics are not severely affected by it.

The calculations show that for small-amplitude sinusoidal waves, there is no recirculation under the wave crests, and that the mean flow velocity is not much different from that of a smooth film of the same mean film thickness. In the case of large-amplitude sinusoidal wave, the mean flow velocity, and thus the Reynolds number of the flow, increase for the same mean film thickness. This would correspond to the experimental observation [34] that upon the onset of wavy flow, the mean film thickness decreases as compared to the film thickness in the wave-free region. Although the heat transfer coefficient still corresponds to that given by the local film thickness, this decrease in the effective film thickness gives rise to an enhancement in the heat transfer coefficient. In the case of solitary waves, their large amplitude has two consequences: firstly, a large recirculation zone develops under these waves; and secondly, since the flow cross-sectional area is much higher under the wave than in the substrate, the mean velocity and the recirculation velocity are small. The contribution of recirculation to heat transfer rate is small, and the overall heat transfer coefficient is still dominated by the conduction process through the inter-wave substrate region. Since most of the fluid is transported in these large waves, the substrate film is thinner and the effective heat transfer coefficient therefore higher. The

effect of waves on heat transfer in thin films is therefore an indirect one, and is due to the effective thinning of the film rather than to enhanced convection within the waves.

Acknowledgements—S. Jayanti gratefully acknowledges the financial help he received from the Science and Engineering Research Council during the period of this study.

REFERENCES

1. W. Nusselt, Die oberflaechenkondensateion des Wasserdampfes, *VDI Zeitschrift* **60,** 541–546; 569–575 (1916).
2. G. D. Fulford, The flow liquids in thin films, *Adv. Chem. Engng* **5,** 151–236 (1964).
3. P. L. Kapitza, Wave flow of thin viscous liquid films, *Zhur. Exper. i. Teor. Fiz.* **18,** 3 (1948).
4. P. L. Kapitza, *Collected papers of P. L. Kapitza*, Vol. 2. Macmillan, New York (1964).
5. T. B. Benjamin, Wave formation in laminar flow down an inclined plane, *J. Fluid Mech.* **2,** 554–574 (1957).
6. T. J. Hanratty and A. Hershman, Initiation of roll waves, *AIChE J.* **7,** 488–497 (1961).
7. T. Ishihara, Y. Iwagaki and Y. Iwasa, Wavy flow in open channels, *Trans. Am. Soc. Civil Engrs* **126** (part 1), 548–563 (1961).
8. H. Brauer, Strömung und Wärmeübergang bei Riselfilmen, *Ver. Deut. Ingr. Forshungsheft* **457** (1956).
9. A. M. Binnie, Experiments on the onset of wave formation on a film of water flowing down a vertical plate, *J. Fluid Mech.* **2,** 551–553 (1957).
10. S. Portalski, The mechanism of flow in wetted wall columns, Ph.D. thesis, University of London (1960).
11. A. E. Dukler and O. P. Bergelin, Characteristics of flow in falling liquid films, *Chem. Engng Progr.* **48,** 557–563 (1952).
12. A. E. Dukler, The role of waves in two-phase flow: some new understanding, 1976 Award Lecture. *Chem. Engng Educ.* **XI,** 108–138 (1977).
13. S. Portalski and A. J. Clegg, An experimental study of wave inception on falling liquid films, *Chem. Engng Sci.* **27,** 1257–1265 (1972).
14. E. Stuhlträger, Y. Naridomi, A. Miyara and H. Uehara, Flow dynamics and heat transfer of a condensate film on a vertical wall—1. Numerical analysis and flow dynamics, *Int. J. Mass Transfer* **36,** 1677–1686 (1993).
15. K. J. Chu and A. E. Dukler, Statistical characteristics of thin wavy films, Part II: studies of the substrate and its wavy structure, *AIChE J.* **20,** 695–706 (1974).
16. K. J. Chu and A. E. Dukler, Statistical characteristics of thin way films, Part III: structure of large waves and their resistance gas flow, *AIChE J.* **21,** 583–593 (1975).
17. A. S. Telles and A. E. Dukler, Statistical characteristics of thin, vertical, wavy liquid films, *Ind. Engng Chem. Fundam.* **9,** 412–421 (1970).
18. T. D. Karapantsios, S. V. Paras and A. J. Karabelas, Statistical characteristics of free falling films at high Reynolds numbers, *Int. J. Multiphase Flow* **14,** 1–21 (1989).
19. V. G. Levich, *Physico-Chemical Hydrodynamics*. Prentice-Hall, Englewood Cliffs, NJ (1962).
20. V. Penev, V. S. Krylov, C. H. Boyadjiev and V. P. Vorotilin, Wave flow of thin liquid films, *Int. J. Heat Mass Transfer* **15,** 1395–1406 (1972).
21. R. I. Hirshburg and L. W. Florsheutz, Laminar wavey film flow: Part 1, hydrodynamic analysis, *J. Heat Transfer Trans. ASME* **104,** 452–458 (1982).
22. D. M. Maron and N. Brauner, Interfacial structure of thin falling films: piecewise modelling of waves, *Physico Chem. Hydrodyn.* **6,** 87–113 (1985).
23. D. M. Maron, N. Bruaner and G. F. Hewitt, Flow pattern in wavy thin films: numerical simulation, *Int. Commun. Heat Mass Transfer* **16,** 655–666 (1989).
24. F. K. Wasden and A. E. Dukler, Insights into the hydrodynamics of free falling wavy films, *AICHE J.* **35,** 187–195 (1989).
25. F. K. Wasden and A. E. Dukler, Numerical investigation of large wave interaction on free falling film, *Int. J. Multiphase Flow* **15,** 357–370 (1989).
26. C. Massot, F. Irani and E. N. Lightfoot, Modified description of wave motion in a falling film, *AIChE J.* **12,** 445–455 (1966).
27. C. G. Kirkbride, Heat transfer by condensing vapour on vertical tube, *Trans. Am. Inst. Chem. Engrs* **30,** 170–193 (1934).
28. G. S. Bays and W. H. McAdams, Heat transfer coefficients in falling film heaters: streamline flow, *Ind. Engng Chem.* **29,** 1240–1246 (1937).
29. S. S. Kutateladze and I. I. Gogonin, Heat transfer in film condensation of slowly moving vapour, *Int. J. Heat Mass Transfer* **22,** 1593–1599 (1979).
30. K. R. Chun and R. A. Seban, Heat transfer to evaporating liquid films, *J. Heat Transfer, Trans. ASME* **93,** 391–396 (1971).
31. R. E. Emmert and R. L. Pigford, A study of gas absorption in falling liquid films, *Chem. Engng Progress* **50,** 87–93 (1954).
32. C. Stirba and D. M. Hurt, Turbulence in falling liquid films, *AIChE J.* **1,** 178–184 (1955).
33. N. Brauner and D. M. Maron, Characteristics of inclined thin films, waviness and the associated mass transfer, *Int. J. Heat Mass Transfer* **25,** 99–110 (1982).
34. S. Portalski and A. J. Clegg, Interfacial area increase in rippled film flow on wetted wall columns, *Chem. Engng Sci.* **26,** 773–784 (1971).
35. I. P. Jones, J. R. Knightly, C. P. Thompson and N. S. Wilkes, FLOW3D, a computer code for the prediction of laminar and turbulent flow and heat transfer: Release 1, UKAEA Report no. AERE-R 11825 (1985).
36. C. M. Rhie and W. L. Chow, Numerical study of the turbulent flow past an air foil with trailing edge separation, *AIAA J.* **21,** 1527–1532 (1983).
37. A. D. Burns and N. S. Wilkes, A finite difference method for the computation of fluids in complex three-dimensional geometries, UKAEA Report no. AERE-R 6687 (1987).
38. J. P. van Doormaal and G. D. Raithby, Enhancement of the SIMPLE method for predicting incompressible flows, *Numer. Heat Transfer* **7,** 147–163 (1984).
39. N. S. Wilkes and C. P. Thompson, An evaluation of higher-order upwinding differencing for elliptic flow problems, UKAEA Report no. CSS 137 (1983).
40. L. O. Jones and S. Whitaker, An experimental study of falling liquid films, *AIChE J.* **12,** 525–529 (1971).